JOURNAL OF GENERAL VIROLOGY

RESEARCH ARTICLE

Chiu *et al.*, *Journal of General Virology* 2026;107:002233
DOI 10.1099/jgv.0.002233

MICROBIOLOGY SOCIETY

OPEN ACCESS

SARS-CoV-2 Nsp15 facilitates immune evasion and viral replication by limiting multiple host innate immune pathways, including cGAS–STING

Hsin-Ping Chiu[1,*], Yao Yu Yeo[2,3], Tsoi Ying Lai[1], Chuan-Tien Hung[1], Shreyas Kowdle[1], Griffin D. Haas[1], Sizun Jiang[2,3,4,5,6], Weina Sun[1] and Benhur Lee[1,*]

Abstract

Severe acute respiratory syndrome coronavirus 2 (SARS-CoV-2) nonstructural protein 15 (Nsp15) is a conserved uridine-specific endoribonuclease (EndoU) and is implicated in innate immune evasion, yet its precise molecular mechanism remains incompletely understood. Here, we demonstrate that Nsp15 limits antiviral innate immune responses in part by downregulating the cGAS–STING pathway. To investigate how Nsp15 antagonizes host innate immune responses, we engineered recombinant SARS-CoV-2 bearing WT or EndoU-inactive Nsp15 (H234A). Compared with the WT virus, the Nsp15-H234A mutant exhibited a 2-log decrease in peak viral titres in interferon (IFN)-competent A549-ACE2 cells, but not in their STAT1 knockout counterparts. This attenuation was partially reversed by STING knockout or STING inhibitors, highlighting STING's involvement in Nsp15-driven immune evasion. Transcriptomic analyses revealed the upregulation of IFNs and IFN-stimulated genes in cells infected with the Nsp15-H234A mutant virus. Notably, cGAS and STING transcripts and proteins were suppressed during WT but not mutant virus infections – even in STAT1-deficient cells – suggesting that Nsp15 contributes directly to their downregulation. *In vitro*, Nsp15 targeted cGAS and STING transcripts in an EndoU activity-dependent manner, thereby reducing cGAS–STING-driven IFN-β and NF-κB reporter activation. Infection of Syrian hamsters confirmed that the Nsp15-H234A mutant virus replicated to lower titres in respiratory tissues and elicited stronger expression of innate immune-related genes. Collectively, these findings define a key strategy by which SARS-CoV-2 Nsp15 subverts the cGAS–STING pathway to facilitate viral replication and immune evasion and underscore Nsp15 EndoU activity as a potential target for future coronavirus antiviral or vaccine design.

DATA AVAILABILITY

All data are included in the manuscript and supplementary information. Raw and processed RNA-sequence data are available at NCBI Gene Expression Omnibus (GEO): GSE274310. Sample accession numbers: Mock (8 hpi): GSM8447165, GSM8447166 and GSM8447167; WT (8 hpi): GSM8447168, GSM8447169 and GSM8447170; H234A (8 hpi): GSM8447171, GSM8447172 and GSM8447173; N277A (8 hpi): GSM8447174, GSM8447175 and GSM8447176; Mock (24 hpi): GSM8447177, GSM8447178 and GSM8447179; WT (24 hpi): GSM8447180, GSM8447181 and GSM8447182; H234A (24 hpi): GSM8447183, GSM8447184 and GSM8447185; N277A (24 hpi): GSM8447186, GSM8447187 and GSM8447188.

Received 25 September 2025; Accepted 02 February 2026; Published 25 March 2026
Author affiliations: [1]Department of Microbiology, Icahn School of Medicine, Mount Sinai, New York, NY, USA; [2]Center for Virology and Vaccine Research, Beth Israel Deaconess Medical Center, Harvard Medical School, Boston, MA, USA; [3]Program in Virology, Division of Medical Sciences, Harvard Medical School, Boston, MA, USA; [4]Department of Pathology, Brigham and Women's Hospital, Harvard Medical School, Boston, MA, USA; [5]Department of Pathology, Dana-Farber Cancer Institute, Boston, MA, USA; [6]Broad Institute of Harvard and MIT, Cambridge, MA, USA.
***Correspondence:** Benhur Lee, benhur.lee@mssm.edu; Hsin-Ping Chiu, hsin-ping.chiu@duke-nus.edu.sg
Keywords: severe acute respiratory syndrome coronavirus 2 (SARS-CoV-2); Nsp15; endoribonuclease; cGAS-STING; innate immune evasion.
Abbreviations: ActD, actinomycin D; AUC, area under the curve; BAC, bacterial artificial chromosome; CHX, cycloheximide; COVID-19, coronavirus disease 2019; CoVs, coronaviruses; DGE, differential gene expression; DMEM, Dulbecco's modified Eagle's medium; dpi, days post-infection; GSEA, gene set enrichment analysis; GSVA, gene set variation analysis; hpi, hours post-infection; IBV, infectious bronchitis virus; ISG, IFN-stimulated gene; MHV, mouse hepatitis virus; PAMPs, pathogen-associated molecular patterns; PCA, principal component analysis; PEDV, porcine epidemic diarrhoea virus; PRRs, pattern recognition receptors; RIP, RNA immunoprecipitation; RNA-seq, RNA sequencing; ROS, reactive oxygen species; RT-qPCR, reverse transcription and real-time quantitative PCR; SARS-CoV-2, severe acute respiratory syndrome coronavirus 2; TCA, tricarboxylic acid.
Eight supplementary figures and three supplementary tables are available with the online version of this article.
002233 © 2026 The Authors

This is an open-access article distributed under the terms of the Creative Commons Attribution License. This article was made open access via a Publish and Read agreement between the Microbiology Society and the corresponding author's institution.

INTRODUCTION

Severe acute respiratory syndrome coronavirus 2 (SARS-CoV-2) belongs to the betacoronaviruses and is the causative agent of coronavirus disease 2019 (COVID-19). Previous coronaviruses (CoVs) infecting humans, including HCoV-229E, OC43, HKU1 and NL63, as well as the highly pathogenic severe acute respiratory syndrome coronavirus (SARS-CoV) and Middle East respiratory syndrome coronavirus (MERS-CoV), have resulted in respiratory illnesses ranging from mild to lethal, depending on viral genetic diversity and host-specific factors.

CoVs are enveloped, positive-sense and single-stranded RNA viruses with a genome ~30 kb in length, featuring 5′-capping and 3′-polyadenylation. The viral genome RNA encodes multiple ORFs for translation of nonstructural replicase proteins (Nsp1-16), structural proteins (spike, membrane, envelope and nucleocapsid) and several accessory proteins [1]. Nsp15 is a uridine-specific endoribonuclease (EndoU) that assembles into an active homo-hexamer, with the N-terminal domain mediating oligomerization and the C-terminal domain conferring EndoU activity [2]. *In vitro* cleavage assays demonstrate that SARS-CoV-2 Nsp15 selectively targets the unpaired uridine within structurally unstable RNA and has a preference for purines 3′ of the cleaved uridine [3]. Mouse hepatitis virus (MHV) Nsp15 not only cleaves positive-sense viral RNA with a strong preference for U↓A and C↓A sequences but also targets the 5′ poly(U) tract in negative-sense viral RNA during infection [4, 5]. SARS-CoV-2 Nsp15 preferentially cleaves AU-rich dsRNA through its dsRNA nickase activity [6]. Besides viral targets, porcine epidemic diarrhoea virus (PEDV) Nsp15 degrades porcine TBK1 and IRF3 dependent on its EndoU activity [7].

The host innate immune system plays pivotal roles in sensing viral infection and evoking initial antiviral responses. The IFN-associated responses and the expression of IFN-stimulated genes (ISGs) constitute the major front line of defence. SARS-CoV-2 infection delays and limits IFN and ISG responses, especially at the early stage of viral replication, and this dysregulation of antiviral innate immune responses contributes to the severity of COVID-19 [8, 9]. SARS-CoV-2 has evolved different strategies to interfere with innate immune responses or otherwise co-opt the host cell's machinery to facilitate optimal viral replication [10]. Nsp15 is a conserved antagonist of host innate immunity across CoVs. Nsp15 limits the recognition of viral RNA by cytosolic dsRNA sensors such as MDA5, PKR and OAS, which are integral to the antiviral defence [11, 12]. It also prevents stress granule assembly, apoptosis and ZBP1-mediated necroptosis in macrophages by controlling the accumulation of viral dsRNA intermediates and shortening the poly(U) sequences in viral RNA [4, 12–14]; well-defined pathogen-associated molecular patterns (PAMPs) are sensed by the host pattern recognition receptors (PRRs). Moreover, Nsp15 has been reported to inhibit host translation independently of the PKR–eIF2α pathway [15]. Nsp15 is considered a virulence determinant, as CoVs such as MHV, PEDV and avian infectious bronchitis virus (IBV) engineered to express a catalytically inactive Nsp15 mutant exhibit an attenuated phenotype *in vitro* and *in vivo* [12, 16, 17].

The vast majority of studies on SARS-CoV-2 Nsp15's ability to antagonize type I IFN production and downstream signalling have relied solely on *in vitro* biochemical assays and IFN-β promoter or IFN-stimulated response element reporter assays [18, 19]. Recently, Otter et al. reported that a recombinant SARS-CoV-2 harboring a catalytically inactive Nsp15 mutation had impaired replication kinetics in primary human nasal epithelial cells, accompanied by increased activation of IFN responses and the PKR pathway [20] . Caobi et al. and Chi et al. later demonstrated a similar attenuated phenotype of the EndoU-inactive SARS-CoV-2 *in vivo* [21, 22]. Nevertheless, the molecular mechanism linked to Nsp15 EndoU activity remains underexplored. To better understand the biological significances of SARS-CoV-2 Nsp15 in the context of viral infection, we generated recombinant SARS-CoV-2 viruses with deficient or absent EndoU activity. Here, we elucidated the replication phenotypes and transcriptomic signatures during WT and Nsp15 mutant virus infection and found cGAS and STING as host targets of Nsp15. We further physiologically evaluated the pathogenesis of Nsp15 EndoU-inactive SARS-CoV-2 in hamsters [23].

METHODS

Cell lines, viruses and chemicals

HEK 293T (ATCC, CRL-3216) and Vero E6 (ATCC, CRL-1586) cells were maintained in Dulbecco's modified Eagle's medium (DMEM) supplemented with 10% FBS (R&D Systems) and 1% penicillin-streptomycin (Pen/Strep) (Gibco) at 37 °C with 5% CO_2. Calu-3 cell (ATCC, HTB-55) was maintained in Eagle's minimum essential medium with 10% FBS and 1% Pen/Strep. A549-hACE2 and A549-hACE2/STAT1 knockout cells [24], kindly gifted by Brad R. Rosenberg, MD, PhD, were cultured in DMEM with 10% FBS and 1% Pen/Strep. A549-hACE2/STING knockout cell was generated by transduction of the lentiviral particle bearing human STING gRNA (Addgene, #127640) and selected under 5 μg ml^{-1} of puromycin. STING inhibitors H-151 and SN-011 were purchased from Invivogen and MedChemExpress, respectively. Cycloheximide (CHX) and actinomycin D (ActD) were acquired from Sigma-Aldrich. Poly(I:C) LMW dsRNA was from Invivogen.

Plasmids

Codon-optimized ORFs of Nsp15 from SARS-CoV-2 (Wuhan-Hu-1 strain, GenBank: NC045512), SARS-CoV (Urbani strain, GenBank: AY278741), MERS-CoV (EMC/2012 strain, GenBank: NC019843), HCoV-229E (ATCC VR-740, GenBank: AF304460), HCoV-OC43 (ATCC VR-759, GenBank: AY585228), HCoV-HKU1 (GenBank: NC006577) and HCoV-NL63 (Amsterdam 1 strain, GenBank: NC005831) fused with C-terminal 1× FLAG or 3× FLAG were inserted into the pcDNA5/FRT/TO vector cut by HindIII (New England Biolabs) and XhoI (New England Biolabs) through In-Fusion cloning (Takara Bio). The alanine substitutions (H234A, H249A, K290A, N277A, S293A and Y342A) were generated by site-directed mutagenesis. pcDNA3.1/HA-hcGAS-V5 and pcDNA3.1/HA-hSTING-V5 are provided by Chia-Yi Yu, PhD. Mouse cGAS and STING coding sequences fused with N-terminal HA tag and C-terminal V5 tag were synthesized by Twist Bioscience and further cloned into the pcDNA3.1 vector. pcDNA/Nsp5-FLAG of SARS-CoV-2 is from Adolfo García-Sastre, PhD.

Rescue of recombinant SARS-CoV-2

We acquired the SARS-CoV-2 bacterial artificial chromosome (BAC) with Venus reporter (USA-WA1/2000) from Luis Martinez-Sobrido, PhD [25]. For establishing the Nsp15 mutant BAC, the subcloning strategy was applied. The DNA sequence between Nsp15 and Spike was PCR amplified and cloned into the pCR-Blunt II-TOPO vector (Invitrogen), and the Nsp15 mutations (H234A and N277A) were generated by site-directed mutagenesis. The inserts with H234A or N277A modification and the original BAC were digested by BstBI (New England Biolabs) and BamHI (New England Biolabs) and ligated using T4 DNA ligase (New England Biolabs). About virus rescue, Vero E6 cells (1×10^6 cells per 6-well) were transfected with 4 µg of BAC construct ($Nsp15_{WT}$, $Nsp15_{H234A}$ and $Nsp15_{N277A}$) using 10 µl of Lipofectamine 2000 (Invitrogen). The next day, the regular medium containing transfection mixture was replaced with infection medium (DMEM supplemented with 2% FBS). After monitoring the infection rate by Venus signal until day 5, the culture supernatants designated as seed stocks (P0) were harvested and stored at −80 °C. The recombinant viruses were propagated and titrated in Vero E6 cells using a plaque assay.

Reverse transcription and real-time quantitative PCR

Total RNA was extracted by use of Direct-zol RNA Miniprep Kit (Zymo Research). Equivalent RNA was reverse-transcribed by random hexamer or oligo(dT) primers with LunaScript RT Master Mix Kit (New England Biolabs). qPCR was run with primers targeting specific genes (Tables S1–S3, available in the online Supplementary Material) and Luna Universal qPCR Master Mix (New England Biolabs) at the Bio-Rad CFX96 Real-Time PCR system (Bio-Rad). The relative RNA level of the specific target was normalized with 18S rRNA (for human) or BACT (for hamster) and calculated by the comparative threshold cycle (ΔΔCT) method.

Western blot and antibodies

Cells were lysed by RIPA lysis buffer (Pierce) containing protease inhibitor cocktail (Roche) and phosphatase inhibitor cocktail (Roche). Equivalent amounts of proteins determined by the Protein Assay Dye Reagent (Bio-Rad) were separated by reducing SDS-PAGE and transferred to a PVDF membrane, 0.22 µm (Bio-Rad). To avoid the nonspecific antibody reaction, membranes were blocked with PBS blocking buffer (LI-COR; 927-700001) and then probed with the primary antibodies targeting specific proteins. For secondary antibodies' incubation, the membranes were washed and then treated with anti-mouse or anti-rabbit Alexa Fluor 647-conjugated secondary antibodies (Invitrogen). The fluorescent signals were developed using the ChemiDoc MP imaging system (Bio-Rad). The following primary antibodies were applied: mouse anti-SARS N (clone 1C7), which cross-reacts to SARS-CoV-2 N, was provided by James A. Duty, PhD; rabbit anti-SARS-CoV-2 Nsp15 (GTX135737) from GeneTex; rabbit anti-ACE2 (ab108252), rabbit anti-pPKR (ab32036) and mouse anti-GAPDH (ab8245) from Abcam; rabbit anti-STAT1 (#14994), rabbit anti-peIF2α (#3398), rabbit anti-PKR (#12297), rabbit anti-V5 (#13202), mouse anti-FLAG (#8146) and rabbit anti-COXIV (#4850) from Cell Signaling Technology; rabbit anti-eIF2α (11170-1-AP), rabbit anti-cGAS (26416-1-AP), rabbit anti-STING (19851-1-AP) and rabbit anti-Lamin B1 (12987-1-AP) from Proteintech; and mouse anti-puromycin (MABE343) from Sigma-Aldrich.

Immunoprecipitation

Cells (4 mg of lysates) lysed by RIPA lysis buffer (Pierce) containing protease inhibitor cocktail (Roche) were immunoprecipitated with pre-incubated mixture of 50 µl of protein A/G magnetic beads (Pierce) and 10 µg of anti-SARS-CoV-2 Nsp15 antibody (16820-1-AP, Proteintech) or rabbit IgG (12–370, EMD Millipore) at 4 °C overnight. The antibody-protein complexes were then washed three times with TBS containing 0.05% Tween 20 and eluted by 50 µl of reducing SDS-PAGE sample buffer at room temperature. The pull-down Nsp15 proteins were clarified by Western blot.

RNA immunoprecipitation

Co-immunoprecipitation and reverse transcription and real-time quantitative PCR (RT-qPCR) were combined to examine the interaction between proteins (Nsp5 and Nsp15) and target RNAs (cGAS, STING and 18S rRNA). Cells (2 mg of lysates) lysed

by IP lysis buffer [50 mM Tris HCl (pH 7.4), 150 mM NaCl, 1 mM EDTA and 1% Triton X-100] containing protease inhibitor cocktail (Roche) and RNase inhibitor (Promega) were incubated with 50 µl of anti-DYKDDDK magnetic agarose (Pierce) at 4 °C overnight. The antibody-protein-RNA complex was then washed five times with IP lysis buffer and divided into two portions. One-third of the RNA immunoprecipitation (RIP) complex was eluted with 50 µl of reducing SDS-PAGE sample buffer and boiled at 95 °C for 10 min and then applied for Western blot; the remaining two-thirds was processed for RNA extraction and RT-qPCR.

Reporter assay

HEK293T cells were co-transfected with Firefly luciferase reporter plasmids under control of the IFN-β promoter or NF-κB responsive elements (pGL4.32[luc2P/NF-κB-RE/Hygro], Promega) and pRL-TK control plasmid along with the indicated plasmids including empty vector, cGAS/STING, mCherry and Nsp15 (WT or H234A) for 48 h. Relative luciferase activity (Firefly/Renilla) was performed by use of Dual-Glo Luciferase System (Promega).

Hamster challenge studies

The rSARS-CoV-2 with Venus reporter ($Nsp15_{WT}$ and $Nsp15_{H234A}$) applied for hamster infection were rescued and propagated in Vero-hTMPRSS2 cells [26]. Viral titres were determined in Vero E6 cells using a plaque assay. Nsp15 sequences were validated by Sanger sequencing. Six- to eight-week-old female golden Syrian hamsters (HsdHan:AURA) were purchased from Inotiv. For the challenge, hamsters were anesthetized with a ketamine/xylazine cocktail before administration of 50 µl of total volume split between each nostril. Animals were challenged with 10,000 p.f.u. of each virus. A group of healthy control animals was left untreated. Animals from each group were euthanized at day 5 post-challenge to harvest nasal turbinates, lung lobes, olfactory bulbs and brain. The nasal turbinates, olfactory bulbs, brain and each of the upper right (cranial) and lower right (caudal) lung lobes were homogenized in 1 ml of sterile PBS. Viral titration by plaque assay was performed in Vero E6 cells. The homogenates from the upper right lung lobes were mixed with TRIzol LS reagent (Invitrogen) for the evaluation of host responses by RT-qPCR. Left lung lobes were collected and stored in 4% (v/v) paraformaldehyde solution in PBS (pH 7.4) overnight and later embedded in paraffin as formalin-fixed paraffin-embedded tissue. The Biorepository and Pathology Core at Icahn School of Medicine at Mount Sinai was responsible for the H&E staining for histopathological evaluation.

RNA sequencing and analysis

Total RNA from mock-infected and virus-infected cells was lysed with TRIzol reagent (Invitrogen), then extracted and on-column DNase I treated using Direct-zol RNA Miniprep kit (Zymo Research). RNA samples were delegated to GENEWIZ, lnc. for polyadenylated RNA enrichment, RNA sequencing (RNA-seq) library preparation and sequencing process. Sequencing libraries were sequenced on an Illumina HiSeq platform (2×150 bp, ~350 M paired-end reads). The reference genome was generated by concatenating the hg38 human and rSARS-CoV-2-Venus (termed SC2-Venus) genomes, which was used for aligning fastq reads using STAR (v2.7.11a). Transcript abundances were then quantified using salmon (v1.10.2) and scaled by transcript length and library size using the R package 'tximport' (v1.26.1). Principal component analysis (PCA) was performed using the R package 'stats' (v4.2.1). Differential gene expression (DEG) was performed using the R package 'DESeq2' (v1.38.3); the false discovery rate for Benjamini–Hochberg *P*-value adjustment was set to 0.05. Gene set enrichment analysis (GSEA) was performed by first ranking the DEGs (scored using log2 fold change×adjusted *P*-values) and then using the R package 'fgsea' (v1.24.0) with the default parameters. Gene set variation analysis (GSVA) was performed using the R package 'GSVA' (v1.46.0). The gene signatures used for GSEA (Hallmark) and GSVA (Gene Ontology) were obtained from MSigDB using the R package 'msigdbr' (v7.5.1). For data visualization, Fig. 3(b, d) is generated using the R packages 'ggplot2' (v3.5.0) and 'ggrepel' (v0.9.5), Fig. 3(c) is generated using the R package 'ggvenn' (v0.1.10) and Fig. 3(e, f) is generated using the R packages 'ComplexHeatmap' (v2.14.0) and 'circlize' (v0.4.16).

Statistical analysis

All statistical analyses were calculated by the use of Prism 10 (GraphPad). An unpaired t-test was used to estimate the statistical significance between two groups. One-way and two-way ANOVA were used to estimate the statistical significance among multiple groups or conditions. Representative data are shown as mean±SD or mean±SEM with biological triplicates or quadruplicates. $P \leq 0.05$ was considered statistically significant: *$P \leq 0.05$; **$P \leq 0.01$; ***$P \leq 0.001$; ****$P \leq 0.0001$; NS, not significant.

RESULTS

Attenuation of Nsp15 catalytically mutant SARS-CoV-2 in IFN-competent human lung-derived epithelial cell lines

To investigate the biological functions of SARS-CoV-2 Nsp15 during viral replication, we employed the BAC system to generate recombinant SARS-CoV-2 (rSARS-CoV-2) expressing Venus reporter with two distinct Nsp15 mutations: H234A and N277A (Fig. 1a). The H234A mutation abolishes EndoU activity, whereas N277A manifests lower *in vitro* catalytic activity and specificity for uridine [27, 28]. rSARS-CoV-2 bearing WT and mutant (H234A, N277A) Nsp15

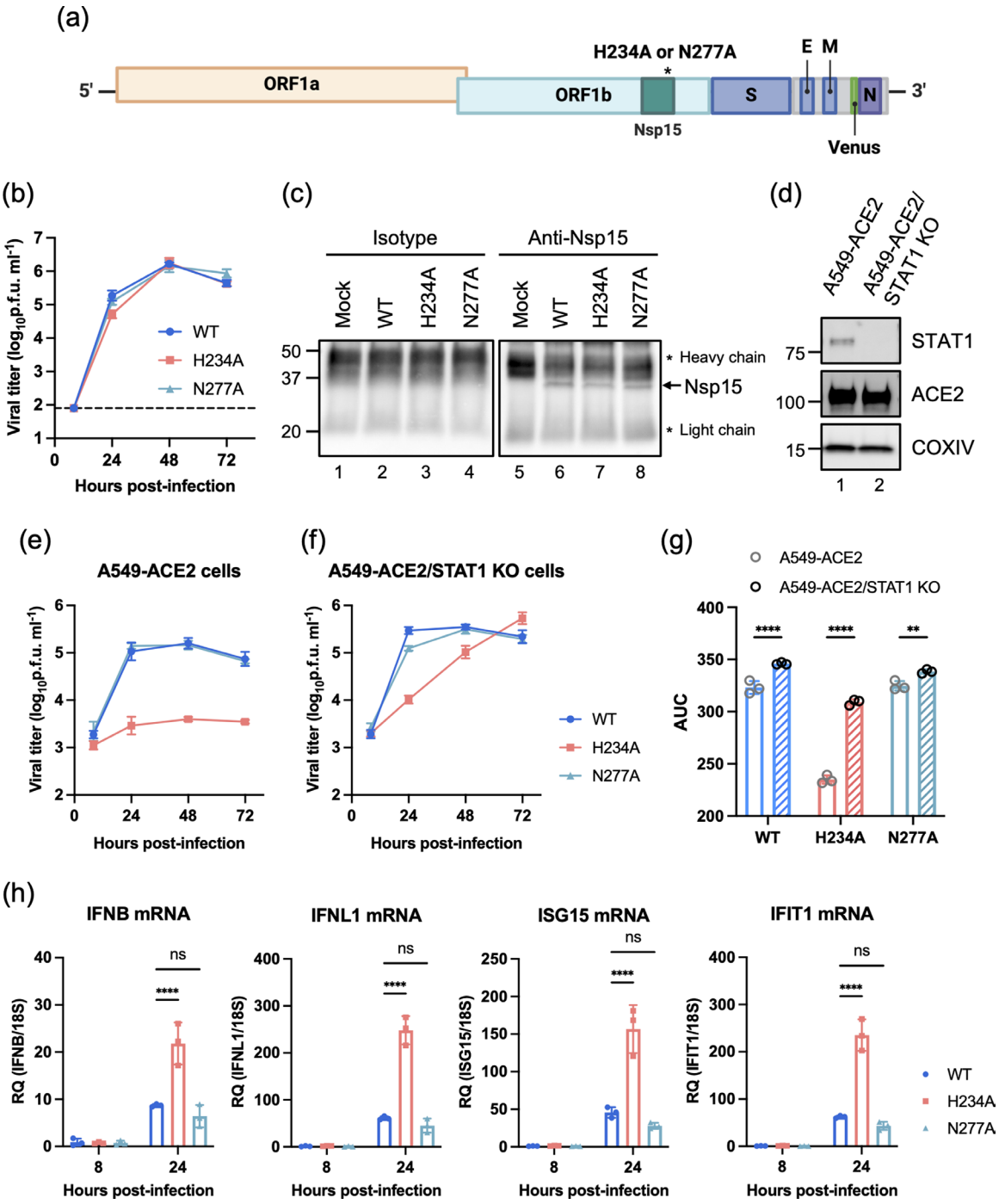


Fig. 1. Infection of Nsp15 WT and mutant SARS-CoV-2 in cell culture. (**a**) Schematic diagram of the recombinant SARS-CoV-2 genome with Nsp15 H234A and N277A mutations. (**b**) Replication kinetics of $Nsp15_{WT}$, $Nsp15_{H234A}$ and $Nsp15_{N277A}$ rSARS-CoV-2 in Vero E6 cells (m.o.i. of 0.001). (**c**) Cell lysates from mock- and virus-infected Vero E6 cells (m.o.i. of 0.001) after 48 h of infection were incubated with anti-Nsp15 antibody or isotype control. Immunoblot analysis was applied for the immunoprecipitated Nsp15 proteins. (**d**) Western blot for ACE2 and STAT1 in A549-ACE2 cells with or without STAT1 knockout. (**e, f**) Replication kinetics of $Nsp15_{WT}$, $Nsp15_{H234A}$ and $Nsp15_{N277A}$ rSARS-CoV-2 in A549-ACE2 and A549-ACE2/STAT1 knockout cells (m.o.i. of 1). (**g**) The AUC was calculated from each viral growth curve and plotted as a bar graph. Data are mean±sd (n=3) and analysed by two-way ANOVA with Šídák multiple comparison test. (**h**) A549-ACE2 cells were uninfected or infected by $Nsp15_{WT}$, $Nsp15_{H234A}$ and $Nsp15_{N277A}$ rSARS-CoV-2 at m.o.i. of 1 for 8 and 24 h. Total RNA was collected for evaluating the host responses by RT-qPCR. Relative gene expression was normalized by 18S rRNA and presented relative to mock infection. Data are mean±sd (n=3) and analysed by two-way ANOVA with Dunnett's multiple comparison test. *P≤0.05; **P≤0.01; ***P≤0.001; ****P≤0.0001; ns, not significant.

replicated equivalently in IFN-deficient Vero E6 cells (Fig. 1b). Immunoprecipitation of infected cell lysates revealed that the H234A and N277A mutants were expressed comparably to WT Nsp15 protein during viral infection (Fig. 1c). To examine the effects of IFN signalling and downstream ISGs on the replication of WT versus mutant Nsp15 viruses, we used A549-ACE2 cells and its isogenic A549-ACE2/STAT1 knockout counterpart that is deficient in IFN signalling [24] (Fig. 1d). Relative to the WT virus, the replication of the $Nsp15_{H234A}$ mutant virus was markedly attenuated in IFN-competent A549-ACE2 cells (Fig. 1e). However, in A549-ACE2/STAT1 knockout cells, $Nsp15_{H234A}$ mutant virus achieved peak titres comparable to WT virus despite a lag at earlier time points (Fig. 1f). Importantly, the replication of each virus was elevated in STAT1 knockout cells, supporting the sensitivity of SARS-CoV-2 to IFN responses, which have been described previously [29–31]. Area under the curve (AUC) analysis of the viral growth trajectories quantified the significantly attenuated phenotype of the $Nsp15_{H234A}$ mutant virus in A549-ACE2 cells and the enhanced replication of each virus in STAT1 knockout cells with the greatest enhancement seen for the $Nsp15_{H234A}$ mutant virus (Fig. 1g). We further validated the defective replication of the $Nsp15_{H234A}$ mutant in Calu-3 cells, a physiologically relevant airway cell line, confirming that the EndoU-associated attenuation is not cell line-specific (Fig. S1A). Together, these results suggest that Nsp15 from SARS-CoV-2 functions as a negative regulator of IFN-mediated antiviral responses.

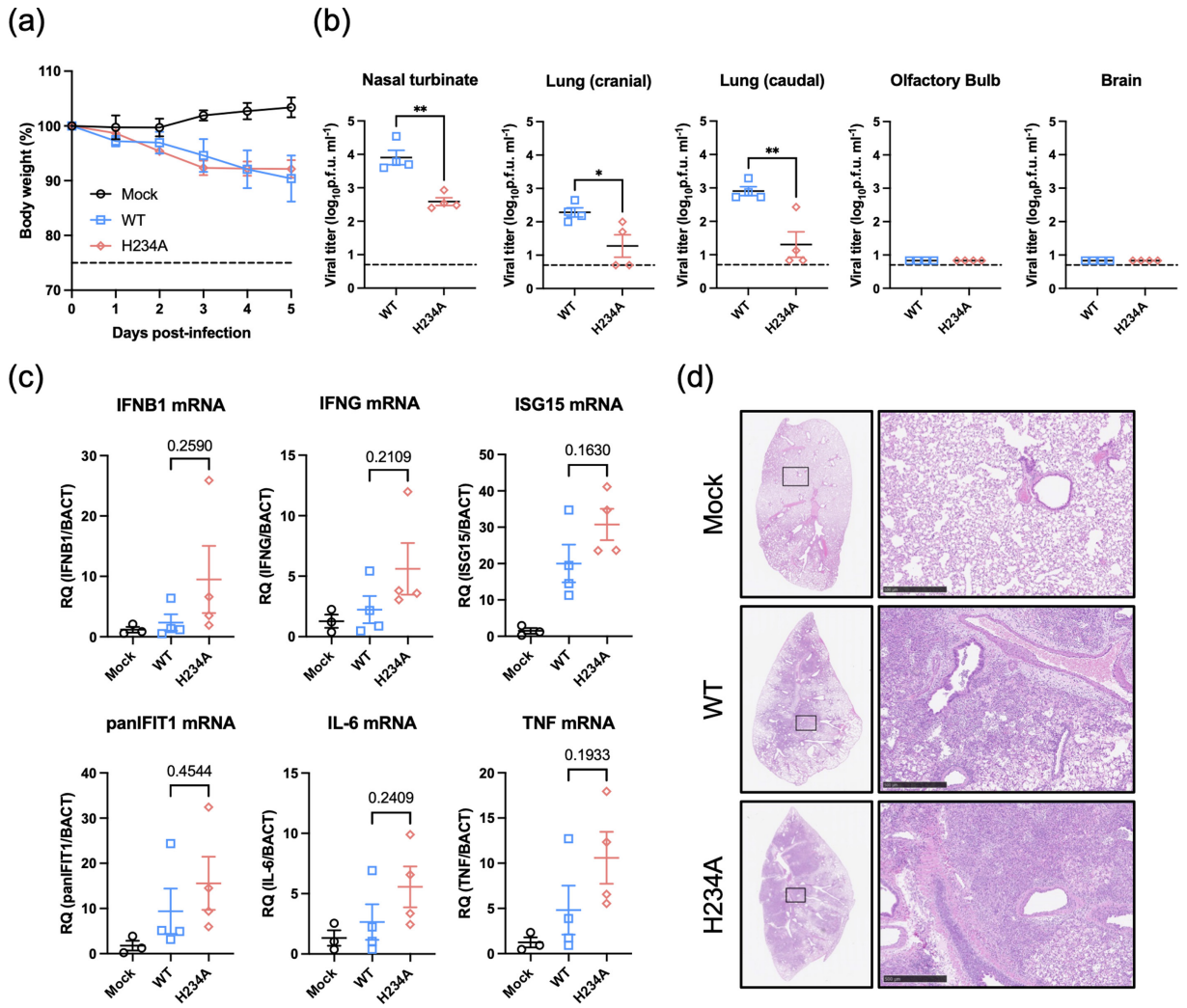


Fig. 2. Viral pathogenesis of Nsp15 EndoU-inactive SARS-CoV-2 in hamsters. Syrian hamsters were intranasally inoculated with 10,000 p.f.u. of $Nsp15_{WT}$ or $Nsp15_{H234A}$ rSARS-CoV-2, or equivalent volume of PBS. (**a**) Body weight change (%) following mock, $Nsp15_{WT}$ and $Nsp15_{H234A}$ virus infection (n=4). (**b**) Viral titre in the nasal turbinates, lungs, olfactory bulbs and brains at 5 dpi, measured by plaque assay. Data are mean±SEM (n=4) and analysed by unpaired t-test. *P≤0.05; **P≤0.01. The dotted line represents the limit of detection. (**c**) Host responses in upper lungs (cranial) at 5 dpi assessed by RT-qPCR. Data are mean±SEM (n=4, except for mock/PBS where n=3). Exact P-values are shown and calculated by a parametric unpaired t-test. (**d**) Lung pathology assessment at 5 dpi performed by H&E staining. Scale bar=500 µm.

Enhancement of innate immune responses during Nsp15$_{H234A}$ SARS-CoV-2 infection

Nsp15 is well-documented to enable the escape of cytosolic dsRNA sensors recognition, including PKR and OAS [32]. The results shown in Fig. 1(e, f) also implicated the importance of IFN-induced signalling pathways in controlling Nsp15$_{H234A}$ mutant replication. Distinct from Nsp15$_{WT}$ and Nsp15$_{N277A}$ viruses, which exhibited similar replication dynamics, Nsp15$_{H234A}$ virus with an attenuated phenotype triggered higher expression of IFNs and ISGs in A549-ACE2 cells (Fig. 1h), implying that the replication defect observed during Nsp15$_{H234A}$ virus infection is a consequence of enhanced host innate immune responses. Additionally, we monitored PKR and eIF2α phosphorylation, as well as rRNA decay, which serve as indicators of PKR and OAS/RNase L activation described previously. At 8 h post-infection (hpi), A549-ACE2 cells infected with Nsp15$_{H234A}$ virus exhibited increased levels of pPKR, peIF2α and degradation of 28S and 18S rRNA compared to those of the other two viruses. However, by 24 hpi, these elevations had subsided, probably reflecting the significant decrease in the replication of the Nsp15$_{H234A}$ mutant (Fig. S1B, C).

Attenuated replication and enhanced innate immune responses of Nsp15 EndoU-inactive SARS-CoV-2 in respiratory tissues of hamsters

Nsp15$_{H234A}$ mutant rSARS-CoV-2 was attenuated in cells with functional IFN-associated responses (Fig. 1). Therefore, we sought to investigate the impact of Nsp15 EndoU activity on viral pathogenesis *in vivo*. We intranasally infected Syrian hamsters with Nsp15$_{WT}$ and Nsp15$_{H234A}$ rSARS-CoV-2 and subsequently monitored for body weight change, viral loads in tissues and host responses, respectively. As expected, mock-infected hamsters slightly gained weight over time; but surprisingly, hamsters infected with WT or Nsp15 $_{H234A}$ virus lost similar weight by 5 days post-infection (dpi) (Fig. 2a). Despite the similar clinical manifestations between WT and Nsp15 $_{H234A}$ infection groups, Nsp15$_{H234A}$ virus exhibited lower viral titre in respiratory tissues, such as nasal turbinates and lungs (Fig. 2b), and elicited a stronger trend toward increased innate immune responses in lungs than WT virus at 5 dpi (Fig. 2c). Histopathological analysis of lungs by haematoxylin and eosin staining revealed comparable immune cell infiltration in WT and Nsp15$_{H234A}$ virus-infected animals, relative to mock infection (Fig. 2d). Notably, the degree of weight loss and the severity of lung pathology did not reflect the difference in viral replication, likely because the heightened innate immune responses triggered by the Nsp15$_{H234A}$ mutant contribute to inflammation-driven tissue damage, thereby producing clinical and histopathological outcomes similar to those observed in WT infection. Overall, despite comparable weight loss and lung pathological damage, the Nsp15$_{H234A}$ mutant demonstrated decreased replication and enhanced innate immune responses in the respiratory tract of hamsters, consistent with the phenotypes seen in cell culture (Fig. 1), though the alteration did not translate into a measurable difference in disease severity.

Nsp15 antagonizes host antiviral innate immune responses and dampens cellular metabolism

To gain insight into the host cellular responses modulated by Nsp15 during viral infection, we performed transcriptomic analysis of A549-ACE2 cells with rSARS-CoV-2 harbouring WT, H234A or N277A Nsp15, as well as a mock infection control. Total RNA was harvested at 8 or 24 hpi for poly(A)-enriched bulk RNA-seq (Fig. 3a). PCA revealed that cells infected with the Nsp15$_{H234A}$ virus exhibited a unique transcriptional profile, distinct from both mock-infected cells and cells infected with the other two viruses. In contrast, the transcriptional profiles from Nsp15$_{WT}$ and Nsp15$_{N277A}$ virus infection were closely clustered, implying similar transcriptional gene programmes (Fig. 3b). Differential gene expression (DGE) analysis further revealed that Nsp15$_{H234A}$ mutant induced more robust transcriptional alterations than Nsp15$_{N277A}$ mutant when compared to Nsp15$_{WT}$ virus infection, and the contrast increased from 8 to 24 hpi (Fig. 3c), suggesting the key role of Nsp15 catalytic activity toward divergent gene expression programmes in SARS-CoV-2-infected cells.

We next performed GSEA between Nsp15$_{WT}$ and Nsp15$_{H234A}$ or Nsp15$_{N277A}$ virus-infected cells using the Molecular Signature Database (MSigDB) Hallmark gene sets [33–35]. At 8 hpi, transcripts from Nsp15$_{H234A}$ virus-infected cells were significantly enriched in innate immune (IFN response) and metabolic (oxidative phosphorylation and MYC targets) signatures, but no observable changes were found in Nsp15$_{N277A}$ virus-infected cells (Fig. 3d, left). At 24 hpi, transcripts from Nsp15$_{H234A}$ virus infection were significantly enriched in other metabolic-associated signatures (e.g. mTORC1 signalling and glycolysis), while transcriptional signatures from Nsp15$_{N277A}$ virus-infected cells began to resemble the Nsp15$_{H234A}$ virus infection at 8 hpi (Fig. 3d, right).

We further performed GSVA using antiviral innate immune and cellular metabolism molecular signatures from the MSigDB Gene Ontology gene sets [36]. Antiviral innate immune signatures were consistently higher in Nsp15$_{H234A}$ virus-infected cells at 8 hpi and further elevated at 24 hpi; these pathways were generally lower in Nsp15$_{N277A}$ virus infection and lowest in Nsp15$_{WT}$ virus infection across both time points. Cellular respiration signatures, while highest in mock-infected cells, were less dampened in Nsp15$_{H234A}$ virus-infected cells as compared to Nsp15$_{WT}$ and Nsp15$_{N277A}$ virus-infected cells, and the contrasts were much larger at 24 hpi (Fig. 3e). Our findings suggest that the lack of Nsp15 catalytic activity leads to increased antiviral innate immune responses and decreased disruption of cellular metabolism. Consistent with GSVA data, Nsp15$_{H234A}$ virus infection showed noticeably higher expression of genes associated with key components of cellular respiration and antiviral innate immune responses compared to Nsp15$_{WT}$ or Nsp15$_{N277A}$ virus infection (Fig. 3f). The majority of the upregulated antiviral genes include IFNs, cytokines, chemokines and ISGs, which represent downstream products of well-established PRRs involved in SARS-CoV-2 recognition, such as RIG-I and MDA5 [37–39]. The loss of Nsp15 activity, leading to the

accumulation of viral dsRNA, is expected to potentiate the activation of these RNA-sensing pathways. Intriguingly, *CGAS* and *STING1* were also robustly expressed by 24 hpi. Given that the cGAS–STING pathway is activated during SARS-CoV-2 infection and may correlate with the disease severity [40–42], we thought that this pathway warrants further investigation in the context of Nsp15 deficiency.

Reduction of cGAS and STING during SARS-CoV-2 infection

Motivated by our RNA-seq findings indicating that cGAS and STING may be regulated by Nsp15 (Fig. 3f), we first look over their endogenous expression in virus-infected cells. After infection for 24 h, A549-ACE2 cells infected with $Nsp15_{WT}$ rSARS-CoV-2 showed significantly reduced cGAS and STING mRNA and protein levels compared to cells infected with the catalytically inactive $Nsp15_{H234A}$ mutant (Fig. 4a). Because cGAS and STING are IFN-inducible, their elevated expression in the $Nsp15_{H234A}$ mutant condition could reflect (i) an indirect effect of enhanced IFN responses, (ii) an inability of the mutant enzyme to directly degrade or regulate the host transcripts or (iii) both.

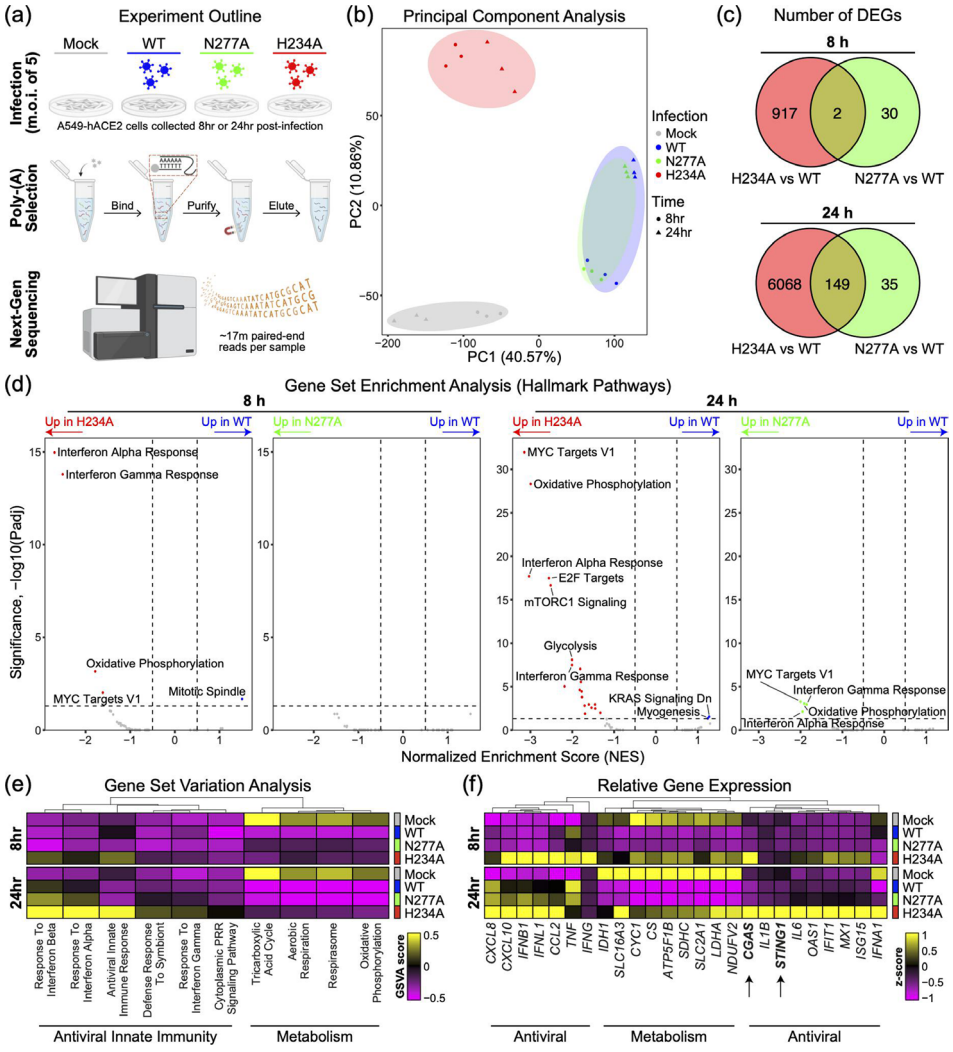


Fig. 3. The global transcriptional signatures from Nsp15 WT and mutant SARS-CoV-2-infected A549-ACE2 cells. A549-ACE2 cells with mock, $Nsp15_{WT}$, $Nsp15_{H234A}$ and $Nsp15_{N277A}$ rSARS-CoV-2 infection for 8 and 24 h (m.o.i. of 5). Total RNA with poly(A) enrichment followed by RNA-seq analysis. (**a**) Schematic of bulk RNA-seq experimental design (n=3 per group). (**b**) PCA of total normalized transcript abundance from mock, Nsp15 WT and mutant rSARS-CoV-2 infection. Sparse PCA depicts the global transcriptome of an individual sample. (**c**) Venn diagram for unique and shared differentially expressed genes (Padj<0.05 and |log2FC|>1) in cells infected with $Nsp15_{H234A}$ and $Nsp15_{N277A}$ mutants compared to $Nsp15_{WT}$ virus. (**d**) Volcano plots showing GSEA results generated using MSigDB Hallmark pathways. (**e**) Cluster heatmap of GSVA scores generated using representative innate immune and metabolic signatures from MSigDB Gene Ontology signatures. (**f**) Expression heatmap of representative innate immune and metabolic genes across mock, WT and mutant rSARS-CoV-2 infection.

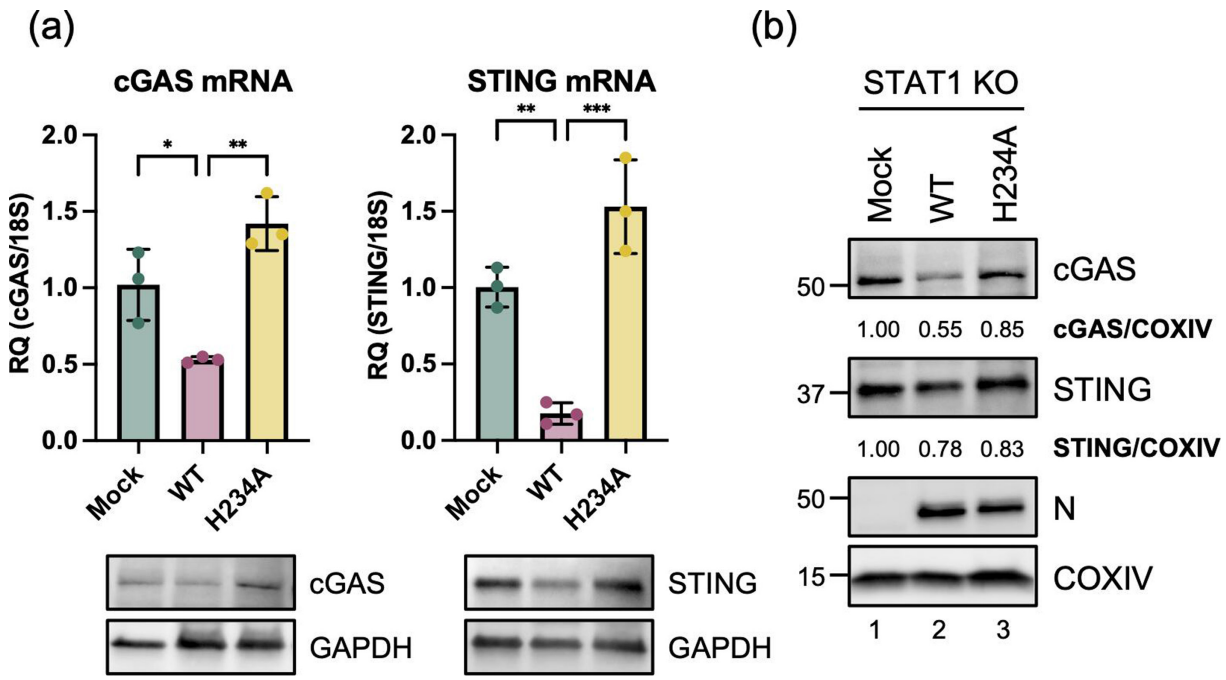


Fig. 4. Decrease in cGAS and STING during SARS-CoV-2 infection. (a) Endogenous cGAS and STING mRNA and protein levels in A549-ACE2 cells uninfected or infected with $Nsp15_{WT}$ and $Nsp15_{H234A}$ rSARS-CoV-2 at m.o.i. of 5 for 24 h. RT-qPCR results are presented relative to the expression of 18S rRNA. Data are mean±SD (n=3) and analysed by one-way ANOVA with Tukey's multiple comparison test. *P≤0.05; **P≤0.01; ***P≤0.001. (b) Endogenous cGAS and STING protein levels in mock, $Nsp15_{WT}$ and $Nsp15_{H234A}$ rSARS-CoV-2 (m.o.i. of 5) infected A549-ACE2/STAT1 knockout cells at 24 hpi.

To ascertain whether Nsp15 influences cGAS/STING levels in a setting with defective IFN-mediated responses, we performed virus infections in A549-ACE2/STAT1 knockout cells. Even in the STAT1-depleted background, $Nsp15_{WT}$ virus reduced endogenous cGAS protein by ~45% relative to mock-infected cells, whereas cGAS was only ~15% lower in $Nsp15_{H234A}$ virus-infected cells (i.e. a 30% difference between $Nsp15_{WT}$ and $Nsp15_{H234A}$ virus infections). The expression of STING was also diminished by the $Nsp15_{WT}$ virus, although more moderately (~22%) and almost not at all (~6%) relative to mock- and $Nsp15_{H234A}$ virus-infected cells, respectively (Fig. 4b). Thus, even in the absence of robust STAT1-dependent IFN signalling, catalytically active Nsp15 partially suppresses cGAS and STING. Taken together, these results indicate that Nsp15 antagonizes cGAS/STING levels through both direct (IFN-independent) and indirect (IFN-mediated) mechanisms, culminating in an overall downregulation of these key antiviral regulators during SARS-CoV-2 infection.

Nsp15 dampens cGAS–STING-mediated innate immune responses

To further verify the biological significance of Nsp15 antagonizing the cGAS–STING pathway, we generated A549-ACE2/STING knockout cells to evaluate the impact of endogenous STING on the replication of $Nsp15_{WT}$ versus $Nsp15_{H234A}$ rSARS-CoV-2 viruses (Fig. 5a). While the $Nsp15_{WT}$ virus exhibited equivalent viral replication in A549-ACE2 cells and its STING knockout counterpart, the $Nsp15_{H234A}$ mutant was partially but significantly restored (3-fold) in A549-ACE2/STING knockout cells relative to the expected decrease (50-fold) in parental A549-ACE2 cells (Fig. 5b). To reinforce the phenotypes of WT and mutant viruses observed from the STING knockout cells, we also infected A549-ACE2 cells with $Nsp15_{WT}$ and $Nsp15_{H234A}$ rSARS-CoV-2 in the presence or absence of STING inhibitors, H-151 or SN-011, chosen for their distinct mechanisms of STING inhibition. H-151 is known to inhibit STING palmitoylation, and SN-011 blocks the cyclic dinucleotide-binding pocket of STING [43, 44]. Under STING inhibitor treatment, $Nsp15_{H234A}$ viral replication was enhanced by 10–20-fold, whereas $Nsp15_{WT}$ viral titre remained unaffected (Fig. S2A, B, red versus blue lines). Both viral infections were performed using a range of inhibitor concentrations that were non-cytotoxic (Fig. S2A, B, black dot line). Treatment with STING inhibitors showed more pronounced rescue effect on the $Nsp15_{H234A}$ mutant virus than that in the cells with STING knockout. Fig. S2C and the previous studies revealed H-151 and SN-011 did not inhibit poly(I:C) or other non-cGAS–STING ligand-triggered IFN-β responses [43, 44]. However, high doses of H-151 and SN-011 appeared to moderately reduce (~50%) exemplar ISGs such as IFIT1 and MX1 (Fig. S2D, E). These data imply that H-151 and SN-011 may possess unknown but beneficial off-target effects that might account for their greater ability to rescue $Nsp15_{H234A}$ virus replication. Altogether, the partially rescued phenotypes observed across distinct approaches indicate that cGAS–STING contributes to restricting the $Nsp15_{H234A}$ virus, while additional PRRs participate in limiting its replication.

cGAS–STING is an intracellular DNA-sensing pathway that drives innate immune responses [45]. However, this pathway is also known to restrict RNA virus infection, probably due to mitochondrial or nuclear DNA leakage during viral infection [46–48]. To ascertain if Nsp15 also inhibits cGAS–STING-induced innate immune responses, we performed IFN-β and NF-κB reporter assays. In the presence of vector control, $Nsp15_{WT}$ did not alter reporter activity; with cGAS–STING stimulation, $Nsp15_{WT}$ significantly reduced IFN-β and NF-κB reporter activity by >75% and >95%, respectively, compared with mCherry control and $Nsp15_{H234A}$ (Fig. 5c, d). To determine if Nsp15-mediated degradation of IFN-β- and NF-κB-driven reporter mRNAs (Fluc) could account for the decrease in reporter activity seen, we conducted RT-qPCR on IFN-β-Luc, NF-κB-Luc and Rluc mRNAs in cells co-transfected with mCherry or WT Nsp15 (Fig. S3A-S3C). Nsp15 appeared to diminish the IFN-β-Luc mRNA by 50% (Fig.

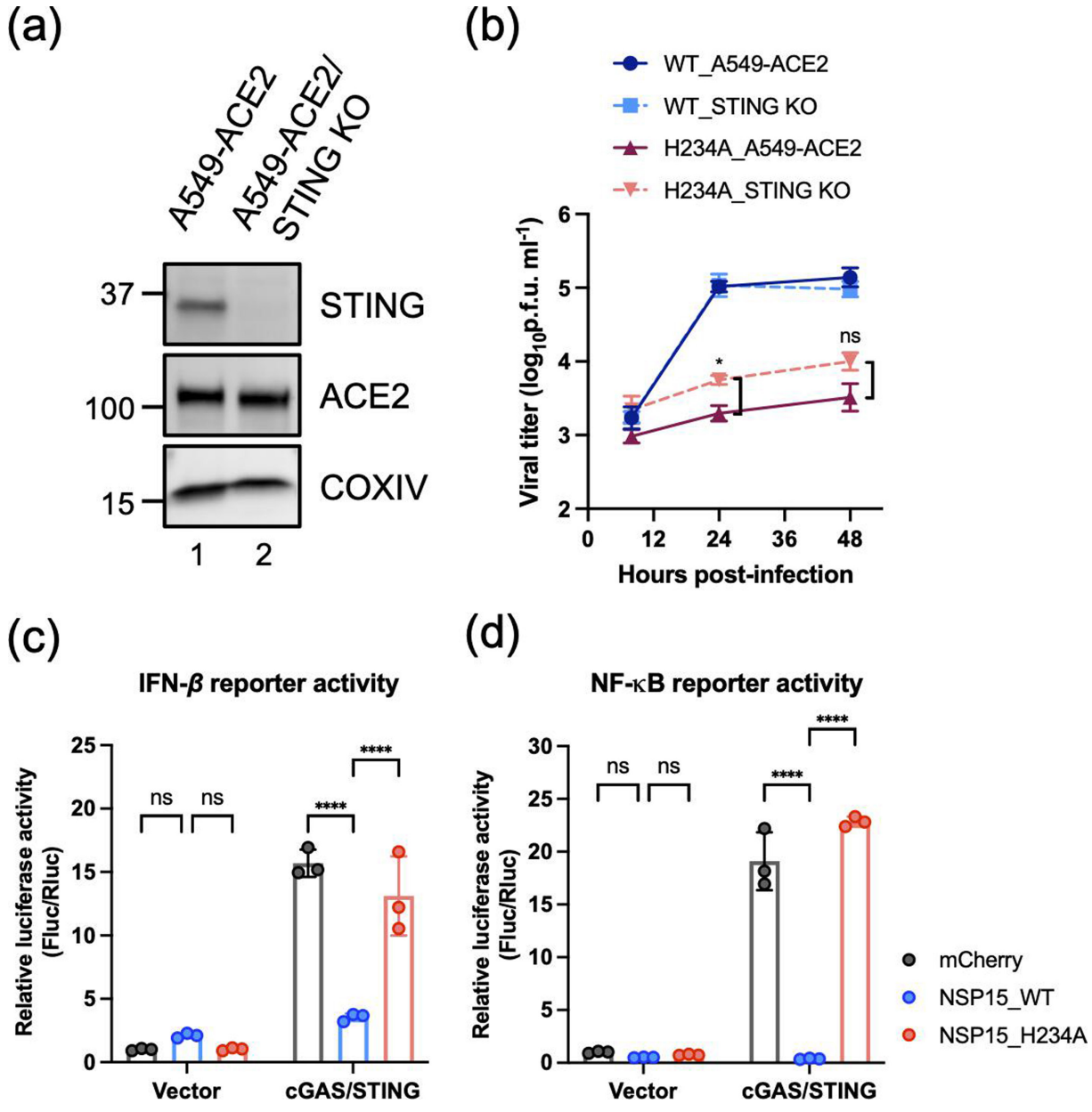


Fig. 5. Inhibition of host cGAS–STING pathway by Nsp15. (a) Western blot for ACE2 and STING in A549-ACE2 cells with or without STING knockout. (b) Replication kinetics of $Nsp15_{WT}$ and $Nsp15_{H234A}$ rSARS-CoV-2 (m.o.i. of 1) in A549-ACE2 and A549-ACE2/STING knockout cells. Viral supernatants collected at individual time points for titration by plaque assay. Data are mean±SD (n=3) and analysed by two-way ANOVA with Tukey's multiple comparison test. (c, d) HEK293T cells were co-transfected with IFN-β promoter reporter plasmid (c) or NF-κB responsive element reporter plasmid (d), Renilla control plasmid plus the indicated plasmids containing empty vector, cGAS/STING, mCherry and WT and H234A Nsp15 for 48 h. Relative luciferase activity was performed by use of Dual-Glo Luciferase System. Data are mean±SD (n=3) and analysed by two-way ANOVA with Tukey's multiple comparison test.

S3A) but had less effect (25% decrease) on the NF-κB-Luc mRNA (Fig. S3B). Intriguingly, there is a net decrease of 121 uridine residues spread across the NF-κB-Luc coding sequence relative to IFN-β-Luc due to differential codon optimization (Fig. S3D). This reduction in uridines in the NF-κB-Luc might account for its increased resistance to Nsp15-mediated cleavage. In either case, any degradation of reporter mRNAs did not appear sufficient to account for the magnitude of reduction seen in IFN-β and NF-κB reporter activity (Fig. 5c, d).

Nsp15 EndoU activity is required for cGAS and STING degradation

The catalytic triad of SARS-CoV-2 Nsp15 (H234, H249 and K289) and residues involved in uridine specificity (N277, S293 and Y342) have been delineated and characterized through structural and biochemical analyses [27, 28] (Fig. S4). To probe the role of these residues in Nsp15's ability to mediate cGAS and STING downregulation, we co-transfected WT and the cognate Nsp15 mutant plasmids along with cGAS or STING plasmid into HEK293T cells and measured RNA and protein levels of cGAS and STING. The mutations located in the RNase catalytic triad (H234A, H249A and K289A) abrogated the downregulation of cGAS and STING, consistent with the published structural and functional characterizations of SARS-CoV Nsp15 [49, 50]. N277A and S293A, the mutations involved in uridine discrimination, retained Nsp15's EndoU activity targeting cGAS and STING (Figs 6a, b and S5). Interestingly, S293A was considered a loss-of-function mutation based on an *in vitro* RNA cleavage assay [28]; in our hands, the impact of S293A is comparable to that of N277A, which was previously defined to have lower EndoU activity and uridine specificity *in vitro* but does not appear to have as dramatic effects as the catalytically inactive mutations [21, 28]. Consistent with these findings, WT Nsp15 also downregulated mouse cGAS and STING (Fig. S6), indicating that the regulatory activity of Nsp15 is not restricted to human cellular targets and may extend across host species.

To evaluate the RNA-binding capacity of Nsp15, we co-transfected HEK293T cells with Nsp5 and Nsp15 plasmids together with cGAS and STING plasmids, followed by RIP assay to determine the protein-RNA interaction. Nsp15 showed enriched binding to cGAS and STING mRNA relative to Nsp5, the main viral protease without RNA-binding potential, implying specific and functional interaction (Fig. 6c, d). To assess the target mRNA stability, we treated HEK293T cells with actinomycin D (ActD) and monitored endogenous cGAS and STING mRNA decay in the presence of WT or H234A Nsp15. In Fig. 6(e), mRNA abundance significantly dropped in WT Nsp15-expressing cells starting from 2 h post-treatment, whereas it was preserved in cells expressing mCherry control or H234A Nsp15. Taken together, these results indicate that SARS-CoV-2 Nsp15 targets and further degrades cGAS and STING mRNAs.

Given that IBV Nsp15 has been reported to suppress host protein synthesis via a PKR–eIF2α-independent mechanism [15], we also investigated whether SARS-CoV-2 Nsp15 exhibits a similar activity. Puromycin pulse-chase assays were performed to monitor nascent protein synthesis. As expected, cycloheximide (CHX), a translation inhibitor, -treated cells exhibited lower incorporation of puromycin into newly synthesized proteins, confirming the feasibility of the assay [51]. HEK293T cells expressing WT Nsp15 only reduced protein synthesis levels by 25% compared to those expressing mCherry at 48 h post-transfection, while cells expressing H234A Nsp15 even showed slightly increased protein synthesis at both 24 and 48 h post-transfection (Fig. S7). Our findings suggest that, different from IBV Nsp15, SARS-CoV-2 Nsp15 does not strongly inhibit host translation, consistent with the prior observation [15].

Divergent activity of Nsp15 targeting cGAS and STING from human CoVs

Currently identified human CoVs, belonging to either alpha- or betacoronavirus lineages, have variable Nsp15 sequence identity (Fig. S8). To extend the inspection for Nsp15 from other human CoVs targeting cGAS and STING, we generated the Nsp15 constructs for SARS-CoV, MERS-CoV, OC43, HKU1, 229E and NL63. These FLAG-tagged Nsp15 displayed variable levels of expression that did *not* correlate with their ability to downregulate cGAS and STING (Fig. 7a, b). Among them, Nsp15 from 229E appeared to have the strongest suppressive activity despite the lowest expression level. Conversely, Nsp15 from SARS-CoV-2 (SARS2 in the figure), expressed much better than that of SARS-CoV and OC43, did not result in greater suppression of cGAS and STING. To determine whether the greatest inhibitory effect from 229E Nsp15 was also enzymatically dependent, we introduced the H235A mutation, a corresponding mutation to the H234A mutation in SARS-CoV-2 Nsp15. Similar to the catalytically inactive SARS-CoV-2 Nsp15, the EndoU-deficient 229E Nsp15 lost its ability to target cGAS and STING (Fig. 7c). Collectively, we posit that our results suggest Nsp15 from different human CoVs may possess distinct substrate selectivity or enzymatic activity.

DISCUSSION

Virus infections trigger host innate and adaptive immunity to counteract the spread of foreign pathogens. Meanwhile, viruses evolve diverse strategies to escape or even manipulate these host defences. CoV Nsp15, while dispensable for viral survival, significantly affects viral replication and virulence *in vitro* and *in vivo*, as demonstrated in studies on animal CoVs, such as MHV, PEDV and IBV [12, 16, 17]. Here, we explore the role of SARS-CoV-2 Nsp15 by employing recombinant viruses with functional impairments in the Nsp15 protein. Inactivation of Nsp15 results in viral attenuation by enhancing host innate

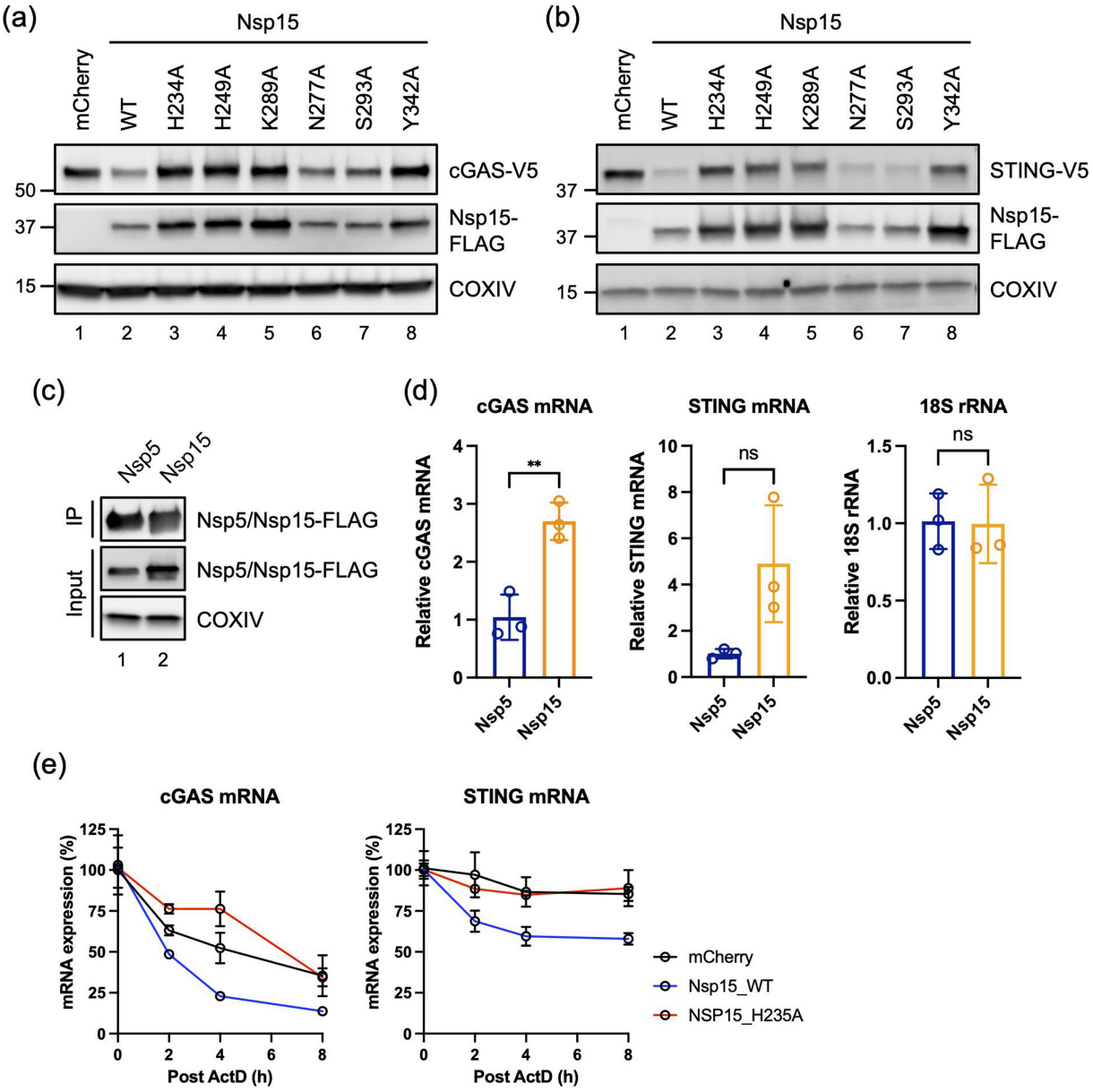


Fig. 6. Role of Nsp15 EndoU activity in cGAS and STING downregulation. (a, b) HEK293T cells were transfected with cGAS or STING plasmid along with WT and mutant SARS-CoV-2 Nsp15 plasmids for 48 h. Protein levels of cGAS (a) and STING (b) were measured by Western blot. (c, d) HEK293T cells were transfected with cGAS and STING plasmids along with SARS-CoV-2 Nsp5-FLAG or Nsp15-FLAG plasmids. After 24 h, total cell lysates were collected and incubated with anti-DYKDDDDK magnetic agarose to pull down the FLAG-tagged proteins and interacting RNAs. (c) Western blot assay of the immunoprecipitated and input Nsp5 and Nsp15 proteins. (d) The Nsp5 and Nsp15-binding cGAS, STING and 18S RNA were quantified using RT-qPCR. The target RNA levels were presented as the fold change in the Nsp15 group relative to the Nsp5 control. Data are mean±SD (n=3) and analysed by unpaired t-test. $^{**}P \leq 0.01$; NS, not significant. (e) HEK293T cells transfected with mCherry, WT or H234A Nsp15 plasmids for 48 h were treated with actinomycin D (5 µg ml^{-1}). Samples were collected at the designated time points post-treatment to monitor the stability of cGAS and STING mRNAs using RT-qPCR. Data are mean±SD (n=3) and shown as relative mRNA expression compared to the starting point (0 h, without ActD).

immune responses (Figs 1, 2 and S1). We also found that the host cGAS–STING pathway is a likely target of Nsp15 and plays a supportive role in the innate immune responses against SARS-CoV-2.

Previous studies have uncovered that SARS-CoV-2 Nsp15 helps to mediate escape from innate immune surveillance, consistent with the known properties of other CoV Nsp15 proteins [32]. Recently, Otter et. al. and Caobi et. al. demonstrated in primary nasal epithelial cells and iPSC-differentiated alveolar type II epithelial (iAT2) cells that rSARS-CoV-2 with an enzymatically dead Nsp15 was more sensitive to IFN-associated viral attenuation than its WT counterpart [20, 21]. Nsp15

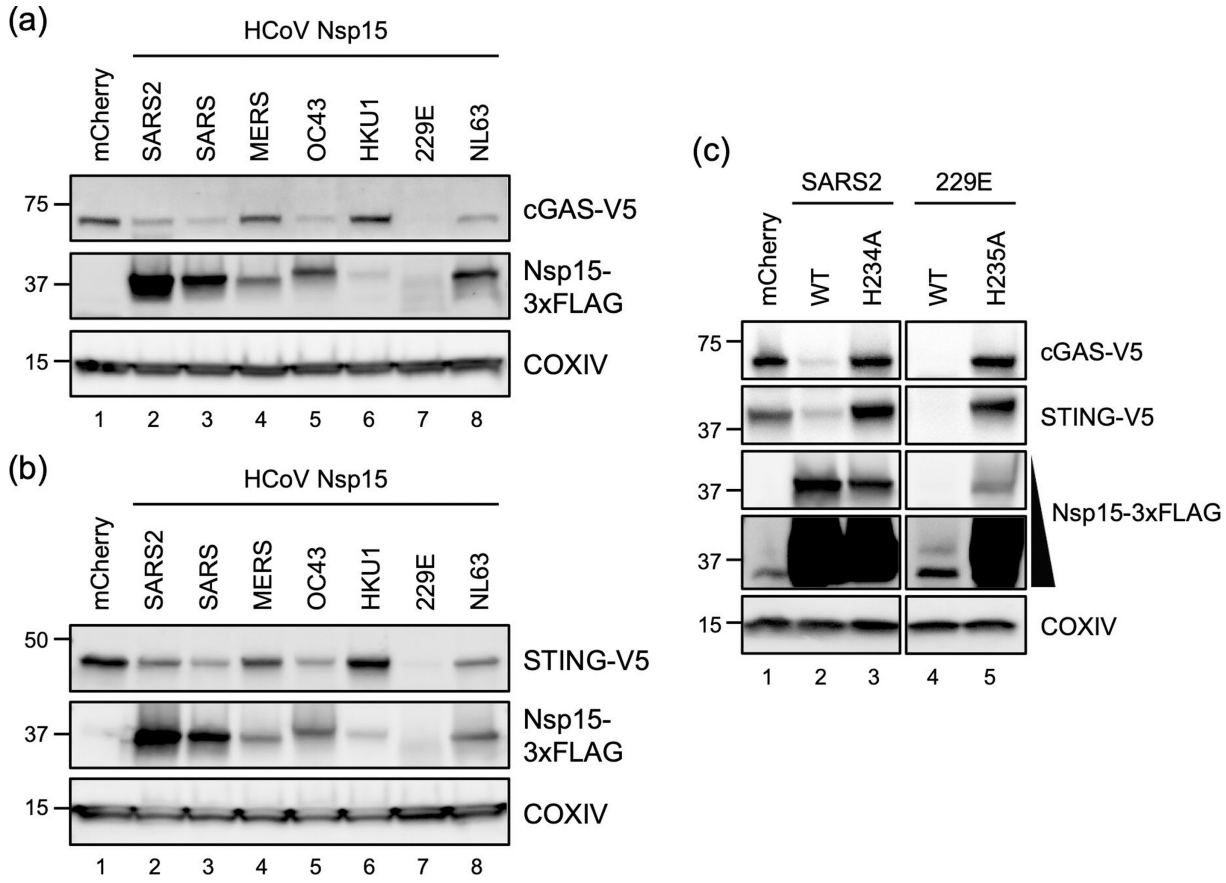


Fig. 7. Divergent activity in downregulating cGAS and STING among human CoV Nsp15. (a, b) HEK293T cells were transfected with cGAS or STING plasmid plus mCherry or HCoV Nsp15 plasmids for 48 h. Western blot performed to assess the expression of indicated proteins. (c) Protein analysis of the HEK293T cells transfected with cGAS or STING plasmid along with mCherry, SARS-CoV-2 and HCoV-229E Nsp15 (WT and corresponding EndoU mutant) plasmids for 48 h.

activity-associated viral attenuation was also validated in K18-hACE2 transgenic mice [21, 22]. Similar to MHV, SARS-CoV-2 with mutant Nsp15 fails to control dsRNA accumulation, thereby enhancing IFN responses and PKR activation [20, 52]. However, the specific molecular mechanism driven by Nsp15 EndoU activity remains elusive. While how Nsp15 functions to downregulate viral RNA-derived PAMPs is relatively well-understood, it is not known whether Nsp15-mediated cleavage of specific host transcripts also contributes to dampening of the innate immune responses. Here, we provide a novel perspective that SARS-CoV-2 Nsp15 exerts its EndoU activity to strengthen the resistance of SARS-CoV-2 to host innate immunity in part by downregulating cGAS and STING (Figs 4, 5 and 6).

Upon SARS-CoV-2 infection, the host innate immune system detects external viral components through a range of RNA- and DNA-sensing pathways, initiating antiviral responses. Viral dsRNA intermediates generated during replication are primarily sensed by PRRs such as RIG-I and MDA5. MDA5 is the dominant RNA sensor for SARS-CoV-2, triggering MAVS-dependent signalling and type I/III IFNs [37, 39]. Several ISGs with RNA-binding activity such as PKR, OAS, ZAP and ISG20 also target SARS-CoV-2 genome [53]. Nsp15, which associates with viral RNA and the replication-transcription complex, prevents the accumulation of viral dsRNA and RNA spillover, thereby dampening activation of IFNs and downstream ISGs [32]. Although cGAS and STING are best known as DNA sensors, they also serve as ISGs that become upregulated downstream of the canonical RNA-sensing signalling pathways. In particular, accumulating evidence uncovers that SARS-CoV-2 infection activates the DNA-mediated cGAS–STING pathway indirectly. Viral replication and spike protein-induced cell fusion and syncytia trigger mitochondrial stress and nuclear damage that release host mitochondrial DNA and nuclear DNA into the cytoplasm, where they serve as ligands for cGAS [41, 54, 55]. Activation of the cGAS–STING pathway is seen not only in cell culture infections but also in clinical lung samples from COVID-19 patients [40, 41]. Additionally, high expression of cGAS and STING is linked to severe COVID-19 and long COVID [42]. Our findings now directly extend Nsp15's EndoU activity in ameliorating the antiviral effects of cGAS–STING activation during SARS-CoV-2 infection. Loss of EndoU activity sensitized the virus to this pathway, as STING knockout or pharmacological inhibition (H-151 or SN-011) partially restored

the replication of the attenuated $Nsp15_{H234A}$ mutant (Figs 5b and S2A, B) and SARS-CoV-2 Nsp15 abolished cGAS–STING-mediated IFN and NF-κB activation in an EndoU activity-dependent manner (Fig. 5c, d). Nsp15 specifically targeted and destabilized cGAS and STING mRNAs via its EndoU function, resulting in the decline in protein expression (Figs 6 and S5). Unlike IBV Nsp15, which robustly suppresses host protein synthesis, SARS-CoV-2 Nsp15 displayed only limited capacity in translational shutdown (Fig. S7) [15]. Whether this modest translation inhibition contributes to the observed phenotypes remains to be determined.

Mitochondrial functions and cellular metabolic processes are crucial in regulating innate immune responses. MAVS, located on the outer membrane of mitochondria, mitochondria-associated ER membranes (MAMs) and peroxisomes, acts as a vital adaptor for RIG-I and MDA5-mediated antiviral signalling [56]. Other mitochondrial-localized proteins such as Tom70, MFN1 and MFN2 are also involved in modulating innate immunity [57]. Reactive oxygen species (ROS), a byproduct of oxidative phosphorylation in mitochondria, are closely linked to inflammatory responses and cellular/tissue damage. ROS directly activate NLRP3 inflammasome, triggering inflammatory signalling [58, 59]. Additionally, ROS have an antiviral effect by promoting IFN-λ production in influenza-infected human nasal epithelial cells [60]. Succinate, an intermediate metabolite of the tricarboxylic acid (TCA) cycle, can stabilize HIF-1α and drive proinflammatory gene expression in macrophages [61]. In Fig. 3(d), SARS-CoV-2 infection with viruses bearing $Nsp15_{WT}$ but not $Nsp15_{H234A}$ suppressed mitochondrial metabolic pathways including oxidative phosphorylation (OXPHOS) and TCA cycle. Our findings in terms of mitochondrial metabolism downregulation in $Nsp15_{WT}$ virus-infected cells align with reports that SARS-CoV-2 reduces the expression of OXPHOS genes and proteins in patient samples, hamster model and K18-hACE2 mouse model [62, 63]. Beyond targeting innate immune pathways directly, SARS-CoV-2 Nsp15 may also impair cellular mitochondrial metabolism to strengthen its inhibitory effect on host antiviral innate immunity. How Nsp15's EndoU activity contributes directly to this metabolic dysregulation phenotype remains to be explored.

Evidence from epidemiological and modelling studies also implicates Nsp15's EndoU activity as a contributing factor to SARS-CoV-2 fitness. While most mutations associated with fitness have been ascribed to the spike protein, an analysis of 6.4 million SARS-CoV-2 genomes as of January 2022 computationally predicted that Nsp15-T112I (virus level numbering), a marker for the Omicron variant, was independently associated with increased fitness [64]. Biochemical analysis subsequently displayed that the T113I (ORF level numbering) mutation *gained* a 250% increase in EndoU activity compared to its parental Wuhan isolate sequence. Structural analyses suggest that this mutant enhances Nsp15 hexamer formation and facilitates binding of longer RNA substrates [65]. Analysis of the GSAID database showed that while Nsp15-T112I comprised only 0.74% of sequences in December 2021, it is now present in almost 98% of sequences in June 2024. This is a higher prevalence than Omicron, defining spike mutations such as E484K (90%) and P681R (95%). Conversely, while H234Y, an EndoU-deficient mutant, first appeared in a subclade of Delta [66], it is only detected in 0.18% of all sequences as of June 2024. These epidemiological analyses underscore the biological significance of Nsp15 to SARS-CoV-2 survival.

In conclusion, our findings highlight the importance of SARS-CoV-2 Nsp15 in facilitating viral replication and counteracting cellular innate immune responses such as cGAS–STING. The attenuated replication observed with Nsp15 EndoU-inactive SARS-CoV-2 in hamster respiratory tissues, coupled with the interaction between Nsp15 and host RNA, may offer novel approaches for developing live-attenuated vaccines and antivirals against current and future CoV infection.

Funding information
This work received no specific grant from any funding agency. H-P.C. was supported by Postdoctoral Research Abroad Program from Ministry of Science and Technology, Taiwan (110-2917-I-564-020). G.D.H. is supported by the National Science Foundation Graduate Research Fellowship Program (Grant No. 1842169). Any opinions, findings and conclusions or recommendations expressed in this material are those of the author(s) and do not necessarily reflect the views of the National Science Foundation. S.J. is supported in part by NIH DP2AI171139, P01AI177687, R01AI149672, a Gilead Research Scholars Program in Hematologic Malignancies, a Sanofi iAward, the Bill & Melinda Gates Foundation INV-002704, the Dye Family Foundation and the Bridge Project, a partnership between the Koch Institute for Integrative Cancer Research at MIT and the Dana-Farber/Harvard Cancer Center. W.S. is supported by seed funding from the Department of Microbiology, Icahn School of Medicine at Mount Sinai. B.L. also acknowledges the Ward-Coleman estate for endowing the Ward-Coleman Chairs at the Icahn School of Medicine at Mount Sinai and diverted support from NIH R21AI149033.

Acknowledgements
We thank Drs Brad Rosenberg, Luis Martinez-Sobrido, Adolfo García-Sastre and Chia-Yi Yu for sharing the materials. We thank members of the Lee lab for experimental assistance and feedback on the project. We thank the Jiang lab for helping with bioinformatic analyses. We thank the Sun lab for helping with hamster-related studies.

Author contributions
H-P.C. and B.L. conceived and designed the study. H-P.C., T.Y.L., C-T.H., S.K., G.D.H. and W.S. performed experiments and collected data. Y.Y.Y. conducted the NGS data processing and analysis. H-P.C. and Y.Y.Y. analysed the data and wrote the original draft of the manuscript. S.J., W.S. and B.L. reviewed and edited the manuscript.

Conflicts of interest
S.J. is a co-founder of Elucidate Bio Inc., has received speaking honorariums from Cell Signaling Technology and has received research support from Roche unrelated to this work.

Ethical statement

All the animal experiments were performed in accordance with protocols approved by the Icahn School of Medicine at Mount Sinai (ISMMS) Institutional Animal Care and Use Committee (IACUC). All experiments with live SARS-CoV-2 were performed in the Centers for Disease Control and Prevention (CDC)/US Department of Agriculture (USDA)-approved biosafety level 3 (BSL-3) biocontainment facility of the Global Health and Emerging Pathogens Institute at the ISMMS, in accordance with institutional biosafety requirements.

References

1. V'kovski P, Kratzel A, Steiner S, Stalder H, Thiel V. Coronavirus biology and replication: implications for SARS-CoV-2. *Nat Rev Microbiol* 2021;19:155–170.
2. Deng X, Baker SC. An "Old" protein with a new story: Coronavirus endoribonuclease is important for evading host antiviral defenses. *Virology* 2018;517:157–163.
3. Salukhe I, Choi R, Van Voorhis W, Barrett L, Hyde J. Regulation of coronavirus Nsp15 cleavage specificity by RNA structure. *PLoS One* 2023;18:e0290675.
4. Hackbart M, Deng X, Baker SC. Coronavirus endoribonuclease targets viral polyuridine sequences to evade activating host sensors. *Proc Natl Acad Sci USA* 2020;117:8094–8103.
5. Ancar R, Li Y, Kindler E, Cooper DA, Ransom M, *et al*. Physiologic RNA targets and refined sequence specificity of coronavirus EndoU. *RNA* 2020;26:1976–1999.
6. Wang X, Zhu B. SARS-CoV-2 Nsp15 preferentially degrades AU-rich dsRNA via its dsRNA nickase activity. *Nucleic Acids Res* 2024;52:5257–5272.
7. Wu Y, Zhang H, Shi Z, Chen J, Li M, *et al*. Porcine epidemic diarrhea virus Nsp15 antagonizes interferon signaling by RNA degradation of TBK1 and IRF3. *Viruses* 2020;12:599.
8. Blanco-Melo D, Nilsson-Payant BE, Liu W-C, Uhl S, Hoagland D, *et al*. Imbalanced host response to SARS-CoV-2 drives development of COVID-19. *Cell* 2020;181:1036–1045.
9. Hadjadj J, Yatim N, Barnabei L, Corneau A, Boussier J, *et al*. Impaired type I interferon activity and inflammatory responses in severe COVID-19 patients. *Science* 2020;369:718–724.
10. Minkoff JM, tenOever B. Innate immune evasion strategies of SARS-CoV-2. *Nat Rev Microbiol* 2023;21:178–194.
11. Kindler E, Gil-Cruz C, Spanier J, Li Y, Wilhelm J, *et al*. Early endonuclease-mediated evasion of RNA sensing ensures efficient coronavirus replication. *PLoS Pathog* 2017;13:e1006195.
12. Deng X, Hackbart M, Mettelman RC, O'Brien A, Mielech AM, *et al*. Coronavirus nonstructural protein 15 mediates evasion of dsRNA sensors and limits apoptosis in macrophages. *Proc Natl Acad Sci USA* 2017;114:E4251–E4260.
13. Gao B, Gong X, Fang S, Weng W, Wang H, *et al*. Inhibition of anti-viral stress granule formation by coronavirus endoribonuclease Nsp15 ensures efficient virus replication. *PLoS Pathog* 2021;17:e1008690.
14. Evdokimova M, Feng S, Caobi A, Moreira FR, Jones D, *et al*. Coronavirus endoribonuclease antagonizes ZBP1-mediated necroptosis and delays multiple cell death pathways. *Proc Natl Acad Sci USA* 2025;122:e2419620122.
15. Gong X, Feng S, Wang J, Gao B, Xue W, *et al*. Coronavirus endoribonuclease Nsp15 suppresses host protein synthesis and evades PKR-eIF2α-mediated translation shutoff to ensure viral protein synthesis. *PLoS Pathog* 2025;21:e1012987.
16. Deng X, van Geelen A, Buckley AC, O'Brien A, Pillatzki A, *et al*. Coronavirus endoribonuclease activity in porcine epidemic diarrhea virus suppresses type I and type III interferon responses. *J Virol* 2019;93:e02000-18.
17. Zhao J, Sun L, Zhao Y, Feng D, Cheng J, *et al*. Coronavirus endoribonuclease ensures efficient viral replication and prevents protein kinase R activation. *J Virol* 2021;95:e02103-20.
18. Yuen C-K, Lam J-Y, Wong W-M, Mak L-F, Wang X, *et al*. SARS-CoV-2 Nsp13, Nsp14, Nsp15 and orf6 function as potent interferon antagonists. *Emerg Microbes Infect* 2020;9:1418–1428.
19. Shemesh M, Aktepe TE, Deerain JM, McAuley JL, Audsley MD, *et al*. SARS-CoV-2 suppresses IFNβ production mediated by Nsp1, 5, 6, 15, ORF6 and ORF7b but does not suppress the effects of added interferon. *PLoS Pathog* 2021;17:e1009800.
20. Otter CJ, Bracci N, Parenti NA, Ye C, Asthana A, *et al*. SARS-CoV-2 Nsp15 endoribonuclease antagonizes dsRNA-induced antiviral signaling. *Proc Natl Acad Sci USA* 2024;121:e2320194121.
21. Caobi A, Su C-M, Beusch CM, Kenney D, Darling TL, *et al*. SARS-CoV-2 Nsp15 enhances viral virulence by subverting host antiviral defenses. *Proc Natl Acad Sci USA* 2025;122.
22. Chi X, Liang X, Vaddadi K, Zhang X, Gandikota C, *et al*. SARS-CoV-2 Nsp15 endoribonuclease subverts host defenses to enhance viral fitness in lung cells. *J Virol* 2025;99:e0117525.
23. Chiu H-P, Yeo YY, Lai TY, Hung C-T, Kowdle S, *et al*. SARS-CoV-2 Nsp15 antagonizes the cGAS-STING-mediated antiviral innate immune responses. *Microbiology* 2024. DOI: 10.1101/2024.09.05.611469.
24. Danziger O, Patel RS, DeGrace EJ, Rosen MR, Rosenberg BR. Inducible CRISPR activation screen for interferon-stimulated genes identifies OAS1 as a SARS-CoV-2 restriction factor. *PLoS Pathog* 2022;18:e1010464.
25. Ye C, Chiem K, Park J-G, Silvas JA, Morales Vasquez D, *et al*. Analysis of SARS-CoV-2 infection dynamic *in vivo* using reporter-expressing viruses. *Proc Natl Acad Sci USA* 2021;118.
26. Oguntuyo KY, Stevens CS, Hung CT, Ikegame S, Acklin JA, *et al*. Quantifying absolute neutralization titers against SARS-CoV-2 by a standardized virus neutralization assay allows for cross-cohort comparisons of COVID-19 sera. *mBio* 2021;12:e02492-20. DOI: 10.1128/mBio.02492-20.
27. Pillon MC, Frazier MN, Dillard LB, Williams JG, Kocaman S, *et al*. Cryo-EM structures of the SARS-CoV-2 endoribonuclease Nsp15 reveal insight into nuclease specificity and dynamics. *Nat Commun* 2021;12:636.
28. Frazier MN, Dillard LB, Krahn JM, Perera L, Williams JG, *et al*. Characterization of SARS2 Nsp15 nuclease activity reveals it's mad about U. *Nucleic Acids Res* 2021;49:10136–10149.
29. Lokugamage KG, Hage A, de Vries M, Valero-Jimenez AM, Schindewolf C, *et al*. Type I interferon susceptibility distinguishes SARS-CoV-2 from SARS-CoV. *J Virol* 2020;94:e01410-20.
30. Vanderheiden A, Ralfs P, Chirkova T, Upadhyay AA, Zimmerman MG, *et al*. Type I and type III interferons restrict SARS-CoV-2 infection of human airway epithelial cultures. *J Virol* 2020;94:e00985-20.
31. Shuai H, Chu H, Hou Y, Yang D, Wang Y, *et al*. Differential immune activation profile of SARS-CoV-2 and SARS-CoV infection in human lung and intestinal cells: implications for treatment with IFN-β and IFN inducer. *J Infect* 2020;81:e1–e10.
32. Van Loy B, Stevaert A, Naesens L. The coronavirus Nsp15 endoribonuclease: a puzzling protein and pertinent antiviral drug target. *Antiviral Res* 2024;228:105921.
33. Subramanian A, Tamayo P, Mootha VK, Mukherjee S, Ebert BL, *et al*. Gene set enrichment analysis: a knowledge-based approach for interpreting genome-wide expression profiles. *Proc Natl Acad Sci USA* 2005;102:15545–15550.
34. Liberzon A, Subramanian A, Pinchback R, Thorvaldsdóttir H, Tamayo P, *et al*. Molecular signatures database (MSigDB) 3.0. *Bioinformatics* 2011;27:1739–1740.
35. Liberzon A, Birger C, Thorvaldsdóttir H, Ghandi M, Mesirov JP, *et al*. The Molecular Signatures Database (MSigDB) hallmark gene set collection. *Cell Syst* 2015;1:417–425.
36. Hänzelmann S, Castelo R, Guinney J. GSVA: gene set variation analysis for microarray and RNA-seq data. *BMC Bioinformatics* 2013;14:7.

37. Sampaio NG, Chauveau L, Hertzog J, Bridgeman A, Fowler G, *et al*. The RNA sensor MDA5 detects SARS-CoV-2 infection. *Sci Rep* 2021;11:13638.
38. Thorne LG, Reuschl A-K, Zuliani-Alvarez L, Whelan MVX, Turner J, *et al*. SARS-CoV-2 sensing by RIG-I and MDA5 links epithelial infection to macrophage inflammation. *EMBO J* 2021;40:e107826.
39. Yin X, Riva L, Pu Y, Martin-Sancho L, Kanamune J, *et al*. MDA5 governs the innate immune response to SARS-CoV-2 in lung epithelial cells. *Cell Reports* 2021;34:108628.
40. Neufeldt CJ, Cerikan B, Cortese M, Frankish J, Lee J-Y, *et al*. SARS-CoV-2 infection induces a pro-inflammatory cytokine response through cGAS-STING and NF-κB. *Commun Biol* 2022;5:45.
41. Domizio JD, Gulen MF, Saidoune F, Thacker VV, Yatim A, *et al*. The cGAS-STING pathway drives type I IFN immunopathology in COVID-19. *Nature* 2022;603:145–151.
42. Queiroz MAF, Brito WR dos S, Pereira KAS, Pereira LMS, Amoras E da SG, *et al*. Severe COVID-19 and long COVID are associated with high expression of STING, cGAS and IFN-α. *Sci Rep* 2024;14:4974.
43. Hong Z, Mei J, Li C, Bai G, Maimaiti M, *et al*. STING inhibitors target the cyclic dinucleotide binding pocket. *Proc Natl Acad Sci USA* 2021;118.
44. Haag SM, Gulen MF, Reymond L, Gibelin A, Abrami L, *et al*. Targeting STING with covalent small-molecule inhibitors. *Nature* 2018;559:269–273.
45. Hopfner KP, Hornung V. Molecular mechanisms and cellular functions of cGAS-STING signalling. *Nat Rev Mol Cell Biol* 2020;21:501–521.
46. Jahun AS, Sorgeloos F, Chaudhry Y, Arthur SE, Hosmillo M, *et al*. Leaked genomic and mitochondrial DNA contribute to the host response to noroviruses in a STING-dependent manner. *Cell Rep* 2023;42:112179.
47. Sun B, Sundström KB, Chew JJ, Bist P, Gan ES, *et al*. Dengue virus activates cGAS through the release of mitochondrial DNA. *Sci Rep* 2017;7:3594.
48. Liu H, Zhu Z, Xue Q, Yang F, Li Z, *et al*. Innate sensing of picornavirus infection involves cGAS-STING-mediated antiviral responses triggered by mitochondrial DNA release. *PLoS Pathog* 2023;19:e1011132.
49. Guarino LA, Bhardwaj K, Dong W, Sun J, Holzenburg A, *et al*. Mutational analysis of the SARS virus Nsp15 endoribonuclease: identification of residues affecting hexamer formation. *J Mol Biol* 2005;353:1106–1117.
50. Bhardwaj K, Palaninathan S, Alcantara JMO, Li Yi L, Guarino L, *et al*. Structural and functional analyses of the severe acute respiratory syndrome coronavirus endoribonuclease Nsp15. *J Biol Chem* 2008;283:3655–3664.
51. Schmidt EK, Clavarino G, Ceppi M, Pierre P. SUnSET, a nonradioactive method to monitor protein synthesis. *Nat Methods* 2009;6:275–277.
52. Li Y, Renner DM, Comar CE, Whelan JN, Reyes HM, *et al*. SARS-CoV-2 induces double-stranded RNA-mediated innate immune responses in respiratory epithelial-derived cells and cardiomyocytes. *Proc Natl Acad Sci USA* 2021;118.
53. Sievers BL, Cheng MTK, Csiba K, Meng B, Gupta RK. SARS-CoV-2 and innate immunity: the good, the bad, and the "goldilocks". *Cell Mol Immunol* 2024;21:171–183.
54. Liu X, Wei L, Xu F, Zhao F, Huang Y, *et al*. SARS-CoV-2 spike protein–induced cell fusion activates the cGAS-STING pathway and the interferon response. *Sci Signal* 2022;15.
55. Zhou Z, Zhang X, Lei X, Xiao X, Jiao T, *et al*. Sensing of cytoplasmic chromatin by cGAS activates innate immune response in SARS-CoV-2 infection. *Sig Transduct Target Ther* 2021;6:382.
56. Chen Y, Shi Y, Wu J, Qi N. MAVS: a two-sided CARD mediating antiviral innate immune signaling and regulating immune homeostasis. *Front Microbiol* 2021;12:744348.
57. West AP, Shadel GS, Ghosh S. Mitochondria in innate immune responses. *Nat Rev Immunol* 2011;11:389–402.
58. Swanson KV, Deng M, Ting JP-Y. The NLRP3 inflammasome: molecular activation and regulation to therapeutics. *Nat Rev Immunol* 2019;19:477–489.
59. Billingham LK, Stoolman JS, Vasan K, Rodriguez AE, Poor TA, *et al*. Mitochondrial electron transport chain is necessary for NLRP3 inflammasome activation. *Nat Immunol* 2022;23:692–704.
60. Chu GE, Park JY, Park CH, Cho WG. Mitochondrial reactive oxygen species in TRIF-dependent toll-like receptor 3 signaling in bronchial epithelial cells against viral infection. *Int J Mol Sci* 2023;25:226.
61. Tannahill GM, Curtis AM, Adamik J, Palsson-McDermott EM, McGettrick AF, *et al*. Succinate is an inflammatory signal that induces IL-1β through HIF-1α. *Nature* 2013;496:238–242.
62. Guarnieri JW, Dybas JM, Fazelinia H, Kim MS, Frere J, *et al*. Core mitochondrial genes are down-regulated during SARS-CoV-2 infection of rodent and human hosts. *Sci Transl Med* 2023;15:eabq1533.
63. Li S, Ma F, Yokota T, Garcia G Jr, Palermo A, *et al*. Metabolic reprogramming and epigenetic changes of vital organs in SARS-CoV-2-induced systemic toxicity. *JCI Insight* 2021;6:e145027.
64. Obermeyer F, Jankowiak M, Barkas N, Schaffner SF, Pyle JD, *et al*. Analysis of 6.4 million SARS-CoV-2 genomes identifies mutations associated with fitness. *Science* 2022;376:1327–1332.
65. Wilson IM, Frazier MN, Li JL, Randall TA, Stanley RE. Biochemical characterization of emerging SARS-CoV-2 Nsp15 endoribonuclease variants. *J Mol Biol* 2022;434:167796.
66. Stern A, Fleishon S, Kustin T, Dotan E, Mandelboim M, *et al*. The unique evolutionary dynamics of the SARS-CoV-2 Delta variant. *Infect Dis* 2021. DOI: 10.1101/2021.08.05.21261642.

The Microbiology Society is a membership charity and not-for-profit publisher.

Your submissions to our titles support the community – ensuring that we continue to provide events, grants and professional development for microbiologists at all career stages.

Find out more and submit your article at microbiologyresearch.org